Oceanic Internal-Wave Field: Theory of Scale-Invariant Spectra

YURI V. LVOV

Rensselaer Polytechnic Institute, Troy, New York

KURT L. POLZIN

Woods Hole Oceanographic Institution, Woods Hole, Massachusetts

ESTEBAN G. TABAK

New York University, New York, New York

NAOTO YOKOYAMA

Doshisha University, Kyotanabe, Japan

(Manuscript received 28 August 2008, in final form 28 July 2010)

ABSTRACT

Steady scale-invariant solutions of a kinetic equation describing the statistics of oceanic internal gravity waves based on wave turbulence theory are investigated. It is shown in the nonrotating scale-invariant limit that the collision integral in the kinetic equation diverges for almost all spectral power-law exponents. These divergences come from resonant interactions with the smallest horizontal wavenumbers and/or the largest horizontal wavenumbers with extreme scale separations.

A small domain is identified in which the scale-invariant collision integral converges and numerically find a convergent power-law solution. This numerical solution is close to the Garrett–Munk spectrum. Power-law exponents that potentially permit a balance between the infrared and ultraviolet divergences are investigated. The balanced exponents are generalizations of an exact solution of the scale-invariant kinetic equation, the Pelinovsky–Raevsky spectrum. A small but finite Coriolis parameter representing the effects of rotation is introduced into the kinetic equation to determine solutions over the divergent part of the domain using rigorous asymptotic arguments. This gives rise to the induced diffusion regime.

The derivation of the kinetic equation is based on an assumption of weak nonlinearity. Dominance of the nonlocal interactions puts the self-consistency of the kinetic equation at risk. However, these weakly nonlinear stationary states are consistent with much of the observational evidence.

1. Introduction

Wave–wave interactions in continuously stratified fluids have been a subject of intensive research in the last few decades. Of particular importance is the observation of a nearly universal internal-wave energy spectrum in the ocean, first described by Garrett and Munk (Garrett and Munk 1972, 1975; Cairns and Williams 1976; Garrett and Munk 1979). However, it appears that ocean is too complex to be described by one universal model. Accumulating evidence suggests that there is measurable variability of observed experimental spectra (Polzin and Lvov 2010, manuscript submitted to *Rev. Geophys.*, hereafter PL). In particular, we have analyzed the decades of observational programs, and we have come to the conclusion that the high-frequency–high-wavenumber part of the spectrum can be characterized through simple power-law fits with variable exponents.

It is generally thought (Müller et al. 1986; Olbers 1974, 1976; PL) that nonlinear interactions significantly contribute to determining the background oceanic spectrum, and this belief motivates the investigation of spectral evolution equations for steady balances. A particularly important study in this regard is the demonstration that the Garrett–Munk (GM) vertical wavenumber spectrum

Corresponding author address: Naoto Yokoyama, Department of Aeronautics and Astronautics, Graduate School of Engineering, Kyoto University, Kyoto 606-8501, Japan.
E-mail: yokoyama@kuaero.kyoto-u.ac.jp

DOI: 10.1175/2010JPO4132.1

is stationary and supports a constant downscale energy flux (McComas and Müller 1981) associated with resonant interactions. The accumulating evidence alluded to above suggests there is more to the story.

The purpose of the present study is to lay down a firm theoretical framework that allows a detailed analysis of power-law spectra of internal waves in the ocean. We investigate the parameter space of the possible power laws with a specific focus on extreme scale-separated interactions and their role in dominating spectral transfers. We then use this theoretical framework to interpret the observed oceanic variability.

Because of the quadratic nonlinearity of the underlying fluid equations and dispersion relation allowing three-wave resonances, internal waves interact through triads. In the weakly nonlinear regime, the nonlinear interactions among internal waves concentrate on their resonant set and can be described by a kinetic equation, which assumes the familiar form (Caillol and Zeitlin 2000; Hasselmann 1966; Kenyon 1966, 1968; Lvov and Tabak 2001, 2004; McComas and Bretherton 1977; Milder 1990; Müller and Olbers 1975; Olbers 1974, 1976; Pelinovsky and Raevsky 1977; Pomphrey et al. 1980; Voronovich 1979; Zakharov et al. 1992)

$$\frac{\partial n_{\mathbf{p}}}{\partial t} = 4\pi \int d\mathbf{p}_{12}\left[|V^{\mathbf{p}}_{\mathbf{p}_1,\mathbf{p}_2}|^2 f^{\mathbf{p}}_{\mathbf{p}_1\mathbf{p}_2}\delta_{\mathbf{p}-\mathbf{p}_1-\mathbf{p}_2}\delta_{\omega_{\mathbf{p}}-\omega_{\mathbf{p}_1}-\omega_{\mathbf{p}_2}} - |V^{\mathbf{p}_1}_{\mathbf{p}_2,\mathbf{p}}|^2 f^{\mathbf{p}_1}_{\mathbf{p}_2\mathbf{p}}\delta_{\mathbf{p}_1-\mathbf{p}_2-\mathbf{p}}\delta_{\omega_{\mathbf{p}_1}-\omega_{\mathbf{p}_2}-\omega_{\mathbf{p}}} - |V^{\mathbf{p}_2}_{\mathbf{p},\mathbf{p}_1}|^2 f^{\mathbf{p}_2}_{\mathbf{p}\mathbf{p}_1}\delta_{\mathbf{p}_2-\mathbf{p}-\mathbf{p}_1}\delta_{\omega_{\mathbf{p}_2}-\omega_{\mathbf{p}}-\omega_{\mathbf{p}_1}}\right],$$
$$\text{with} \quad f^{\mathbf{p}}_{\mathbf{p}_1\mathbf{p}_2} = n_{\mathbf{p}_1}n_{\mathbf{p}_2} - n_{\mathbf{p}}(n_{\mathbf{p}_1} + n_{\mathbf{p}_2}). \tag{1}$$

Here $n_{\mathbf{p}} = n(\mathbf{p})$ is a three-dimensional (3D) action spectrum [see Eq. (16)] with wavenumber $\mathbf{p} = (\mathbf{k}, m)$: that is, $\mathbf{k}$ and m are the horizontal and vertical components of $\mathbf{p}$. Action or wave action can be viewed as "number" of waves with a given wavenumber. The frequency $\omega_{\mathbf{p}}$ is given by a linear dispersion relation (12) below. Consequently, wave action multiplied by frequency $\omega_{\mathbf{p}}n_{\mathbf{p}}$ can be seen as quadratic spectral energy density of internal waves. Note that the wavenumbers are oppositely signed variables, whereas the wave frequencies are always positive. The factor $V^{\mathbf{p}}_{\mathbf{p}_1\mathbf{p}_2}$ is the interaction matrix element describing the transfer of wave action among the members of a triad composed of three wave vectors $\mathbf{p} = \mathbf{p}_1 + \mathbf{p}_2$.

Following Kolmogorov's viewpoint of energy cascades in isotropic Navier–Stokes turbulence, one may look for statistically stationary states using scale-invariant solutions to the kinetic Eq. (1). The solution may occur in an inertial subrange of wavenumbers and frequencies that are far from those where forcing and dissipation act and also are far from characteristic scales of the system, including the Coriolis frequency resulting from the rotation of the earth, the buoyancy frequency due to stratification and the ocean depth. Under these assumptions, the dispersion relation and the interaction matrix elements are locally scale invariant. It is natural, therefore, in this restricted domain, to look for self-similar solutions of Eq. (1), which take the form

$$n(\mathbf{k}, m) = |\mathbf{k}|^{-a}|m|^{-b}. \tag{2}$$

Values of a and b for which the right-hand side of Eq. (1) vanishes identically correspond to steady solutions of the kinetic equation and we hope also to statistically steady states of the ocean's wave field. Unlike Kolmogorov turbulence, the exponents that give steady solutions cannot be determined by the dimensional analysis alone (see, e.g., Polzin 2004). This is the case because of multiple characteristic length scales in anisotropic systems.

Before seeking steady solutions, however, one should find out whether the improper integrals[1] in the kinetic Eq. (1) converge. This is related to the question of locality of the interactions: a convergent integral characterizes the physical scenario where interactions of neighboring wavenumbers dominate the evolution of the wave spectrum, whereas a divergent one implies that distant, nonlocal interactions in the wavenumber space dominate.

In the present paper, we demonstrate analytically that the internal-wave collision integral diverges for almost all values of a and b. In particular, the collision integral has an infrared (IR) divergence at 0 (i.e., $|\mathbf{k}_1|$ or $|\mathbf{k}_2| \to 0$) and an ultraviolet (UV) divergence at infinity (i.e., $|\mathbf{k}_1|$ and $|\mathbf{k}_2| \to \infty$). Thus, IR divergence comes from interactions with the smallest wavenumber, and UV divergence comes from interactions with the largest horizontal wavenumber. There is only one exception where the integral converges: the segment with $b = 0$ and $7/2 < a < 4$. The $b = 0$ line corresponds to wave action independent of

[1] Improper integrals have the form $\lim_{b\to\infty}\int_a^b f(x)\,dx$, $\lim_{a\to-\infty}\int_a^b f(x)\,dx$, $\lim_{c\to b^-}\int_a^c f(x)\,dx$, or $\lim_{c\to a^+}\int_c^b f(x)\,dx$. When the limit exists (and is a number), the improper integral is called convergent; when the limit does not exist or is infinite, the improper integral is called divergent.

vertical wavenumbers, $\partial n/\partial m = 0$. Within this segment, we numerically determine a new steady convergent solution to Eq. (1), with

$$n(\mathbf{k}, m) \propto |\mathbf{k}|^{-3.7}. \tag{3}$$

This solution is not far from the large-wavenumber form of the GM spectrum (Garrett and Munk 1972, 1975; Cairns and Williams 1976; Garrett and Munk 1979),

$$n(\mathbf{k}, m) \propto |\mathbf{k}|^{-4}. \tag{4}$$

Alternatively, one can explore the physical interpretation of divergent solutions. We find a region in (a, b) space where there are both IR and UV divergences having opposite signs. This suggests a possible scenario where the two divergent contributions may cancel each other, yielding a steady state. An example of such a case is provided by the Pelinovsky–Raevsky (PR) spectrum (Pelinovsky and Raevsky 1977),

$$n_{\mathbf{k},m} \propto |\mathbf{k}|^{-7/2}|m|^{-1/2}. \tag{5}$$

This solution, however, is only one among infinitely many. The problem at hand is a generalization of the concept of principal value integrals: for a and b, which give opposite signs of the divergences at zero and infinity, one can regularize the integral by cutting out small neighborhoods of the two singularities in such a way that the divergences cancel each other and the remaining contributions are small. Hence, all the exponents that yield opposite-signed divergence at both ends can be steady solutions of Eq. (1). As we will see below this general statement helps to describe the experimental oceanographic data that are available to us. The nature of such steady solutions depends on the particular truncation of the divergent integrals.

So far, we have kept the formalism at the level of the self-similar limit of the kinetic Eq. (1). However, once one considers energy transfer mechanisms dominated by interactions with extreme modes of the system, one can no longer neglect the deviations from self-similarity near the spectral boundaries: the inertial frequency due to the rotation of the earth at the IR end and the buoyancy frequency and/or dissipative cutoffs at the UV end.

For example, we may consider a scenario in which interactions with the smallest horizontal wavenumbers dominate the energy transfer within the inertial subrange, either because the collision integral at infinity converges or because the system is more heavily truncated at the large wavenumbers by wave breaking or dissipation. We will demonstrate that the IR divergence of the collision integral has a simple physical interpretation: the evolution of each wave is dominated by the interaction with its nearest neighboring vertical wavenumbers, mediated by the smallest horizontal wavenumbers of the system. Such a mechanism is called induced diffusion (ID) in the oceanographic literature.

To bring back the effects of the rotation of the earth in Eq. (1), one introduces the Coriolis parameter f there and in the linear dispersion relation. Because we are considering the evolution of waves with frequency ω much larger than f, f can be considered to be small. However, because the interaction with waves near f dominates the energy transfer, one needs to invert the order in which the limits are taken, postponing making $f = 0$ to the end. This procedure gives rise to an integral that diverges like f raised to a negative power smaller than -1 but multiplied by a prefactor that vanishes if either $9 - 2a - 3b = 0$ or $b = 0$. These are the induced diffusion lines of steady-state solutions, found originally in McComas and Müller (1981) as a diffusive approximation to the kinetic equation. This family of stationary states does a reasonable job of explaining the gamut of observed variability. The rigorous asymptotic analysis presented here clearly implies the induced diffusion family of stationary states makes sense only in the IR divergent subdomain of (a, b) space, and we find that the data are located in this subdomain.

The present paper investigates in detail the parameter space (a, b) of a general power-law spectrum (2), compares this parameter space to the ocean observations, and gives possible interpretation. Furthermore, the present study places the previously obtained ID curves (McComas and Müller 1981) and Pelinovsky–Raevsky spectrum (Pelinovsky and Raevsky 1977) into a much wider context. Finally, we present a general theoretical background that we are going to exploit for future studies.

The paper is organized as follows: Wave turbulence theory for the internal wave field and the corresponding kinetic equation are briefly summarized in section 2 along with the motivating observations. We analyze the divergence of the kinetic equation in section 3. Section 4 includes a special convergent power-law solution that may account for the GM spectrum. In section 5, we introduce possible quasi-steady solutions of the kinetic equation that are based on cancellations of two singularities. Section 6 shows that the IR divergence is dominated by induced diffusion, and we compute the family of power-law solutions that arises from taking it into account. We conclude in section 7.

2. Wave turbulence theory for internal waves

a. Background and history

The idea of using wave turbulence formalism to describe internal waves is certainly not new; it dates back to Kenyon (1966, 1968), with calculations of the kinetic equations for oceanic spectra presented in Olbers (1976), McComas and Bretherton (1977), and Pomphrey et al. (1980). Various formulations have been developed for characterizing wave–wave interactions in stratified wave turbulence in the last four decades (Y.V. Lvov, K. L. Polzin, and N. Yokoyama 2007, unpublished manuscript, hereafter LPY; for details, see Caillol and Zeitlin 2000; Hasselmann 1966; Kenyon 1966, 1968; Lvov and Tabak 2001, 2004; McComas and Bretherton 1977; Milder 1990; Müller and Olbers 1975; Olbers 1974, 1976; Pelinovsky and Raevsky 1977; Pomphrey et al. 1980; Voronovich 1979). We briefly discuss the derivation of the kinetic equation and wave–wave interaction matrix elements below in Eq. (15).

The starting point for the most extensive investigations has been a noncanonical Hamiltonian formulation in Lagrangian coordinates (McComas and Müller 1981) that requires an unconstrained approximation in smallness of wave amplitude in addition to the assumption that nonlinear transfers take place on much longer time scales than the underlying linear dynamics. Other work has as its basis a formulation in Clebsch-like variables (Pelinovsky and Raevsky 1977) and a non-Hamiltonian formulation in Eulerian coordinates (Caillol and Zeitlin 2000). Here, we employ a canonical Hamiltonian representation in isopycnal coordinates (Lvov and Tabak 2001, 2004), which, as a canonical representation, preserves the original symmetries and hence conservation properties of the original equations of motion.

Energy transfers in the kinetic equation are characterized by three simple mechanisms identified by McComas and Bretherton (1977) and reviewed by Müller et al. (1986). These mechanisms represent extreme scale-separated limits. One of these mechanisms represents the interaction of two small-vertical-scale, high-frequency waves with a large-vertical-scale, near-inertial (frequency near f) wave and is called induced diffusion (ID). The ID mechanism exhibits a family of stationary states: that is, a family of solutions to Eq. (2). A comprehensive inertial-range theory with constant downscale transfer of energy can be obtained by patching these mechanisms together in a solution that closely mimics the empirical universal spectrum (GM; McComas and Müller 1981). A fundamental caveat from this work is that the interaction time scales of high-frequency waves are sufficiently small at small spatial scales as to violate the assumption of weak nonlinearity.

In parallel work, Pelinovsky and Raevsky (1977) derived a kinetic equation for oceanic internal waves. They also have found the statistically steady-state spectrum of internal waves, Eq. (5), which we propose to call the Pelinovsky–Raevsky spectrum. This spectrum was later found in Caillol and Zeitlin (2000) and Lvov and Tabak (2001, 2004). It follows from applying the Zakharov–Kuznetsov conformal transformation (Zakharov et al. 1992), which effectively establishes a map between the very large and very small wavenumbers. Making these two contributions cancel pointwise yields the solution (5).

Both Pelinovsky and Raevsky (1977) and Caillol and Zeitlin (2000) noted that the solution (5) comes through a cancellation between oppositely signed divergent contributions in their respective collision integrals. A fundamental caveat is that one cannot use conformal mapping for divergent integrals. Therefore, the existence of such a solution is fortuitous.

Here, we demonstrate that our canonical Hamiltonian structure admits a similar characterization: power-law solutions of the form (2) return collision integrals that are, in general, divergent. Regularization of the integral allows us to examine the conditions under which it is possible to rigorously determine the power-law exponents (a, b) in Eq. (2) that lead to stationary states. In doing so, we obtain the ID family.

The situation is somewhat peculiar: We have assumed weak nonlinearity to derive the kinetic equation. The kinetic equation then predicts that nonlocal, strongly scale-separated interactions dominate the dynamics. These interactions have less chance to be weakly nonlinear than regular, ''local'' interactions. Thus, the derivation of the kinetic equation and its self-consistency are at risk. In our subsequent work (LPY), we provide a possible resolution of this puzzle. However, as we will see below, despite this caveat, the weakly nonlinear theory is consistent with much of the observational evidence.

b. Experimental motivation

Power laws provide a simple and intuitive physical description of complicated wave fields. Therefore, we assumed that the spectral energy density can be represented as Eq. (2) and undertook a systematic study of published observational programs. In doing so, we were fitting the experimental data available to us by power-law spectra. We assume that the power laws offer a good fit of the data in the high-frequency, high-wavenumber parts of the spectrum. We do not assume that spectra are given by Garrett–Munk spectrum.

In most instances, vertical wavenumber and frequency power laws were estimated by superimposing best-fit lines on top of one-dimensional spectra. The quoted power laws are the asymptotic relations of these best-fit lines. Fits in the frequency domain included only periods smaller than 10 h, thereby eliminating the inertial peak and semidiurnal tides from consideration. For one-dimensional spectra, there is an implicit assumption that the high-frequency–high-wavenumber spectra are separable. Because both 1D spectra are red, frequency spectra are typically dominated by low-vertical-wavenumber motions, and vertical wavenumber spectra are dominated by low frequencies. Care should be taken to distinguish these results from the high-wavenumber asymptotics of truly two-dimensional spectra. We have included two realizations of two-dimensional displacement spectra in isopycnal coordinates [the Patches Experiment (PATCHEX^2) and the Surface Wave Process Program (SWAPP)]. The quoted power laws in these instances were estimated using a straight edge and χ-by-eye procedure.

Below we list extant datasets with concurrent vertical profile and current meter observations and some major experiments utilizing moored arrays, along with our best estimate of their high-wavenumber, high-frequency asymptotics:

- Site-D (Foffonoff 1969; Silverthorne and Toole 2009): energy spectra are $m^{-2.0}$ and $\omega^{-2.0}$;
- the Frontal Air-Sea Interaction Experiment (FASINEX; Weller et al. 1991; Eriksen et al. 1991): energy spectra are $m^{-2.3}$ and $\omega^{-1.85}$;
- the Internal Wave Experiment (IWEX; Müller et al. 1978): energy spectrum is $-k^{-2.4\pm0.4}\omega^{-1.75}$;
- the Salt Finger Tracer Release Experiment (SFTRE; Schmitt et al. 2005)/Polymode IIIc (PMIII; Keffer 1983): energy spectra are $m^{-2.4}$ and $\omega^{-1.9}$;
- the North Atlantic Tracer Release Experiment (NATRE; Polzin et al. 2003)–subduction (Weller et al. 2004): energy spectra are $m^{-2.55}$ (observed: NATRE^1) or $m^{-2.75}$ (minus vortical contribution: NATRE^2) and $\omega^{-1.35}$;
- PATCHEX^1 (Gregg et al. 1993; Chereskin et al. 2000): energy spectra are $m^{-1.75}$ and $\omega^{-1.65} - \omega^{-2.0}$;
- PATCHEX^2 (Sherman and Pinkel 1991): energy spectrum is $m^{-1.75}\omega^{-1.65} - m^{-1.75}\omega^{-2.0}$;
- the SWAPP experiment (Anderson 1992): energy spectrum is $m^{-1.9}\omega^{-2.0}$.
- the Storm Transfer and Response Experiment (STREX; D'Asaro 1984)/Ocean Storms Experiment (OS; D'Asaro 1995): energy spectra are $m^{-2.3}$ and $\omega^{-2.2}$;
- the Midocean Acoustic Transmission Experiment (MATE; Levine et al. 1986): energy spectra are $-m^{-2.1}$ and $\omega^{-1.7}$; and
- the Arctic Internal Wave Experiment (AIWEX; Levine et al. 1987; D'Asaro and Morehead 1991): energy spectra are $m^{-2.25}$ and $\omega^{-1.2}$.

Two estimates of the NATRE spectrum are provided: NATRE^1 represents the observed spectrum, and NATRE^2 represents the observed spectrum minus the quasi-permanent finestructure spectrum identified in Polzin et al. (2003). The residual (NATRE^2) represents our best estimate of the internal-wave spectrum. Two estimates of the PATCHEX spectrum are provided: PATCHEX^1 combines free-fall vertical profiler data from Gregg et al. (1993) and long-term current meter data from Chereskin et al. (2000), and PATCHEX^2 is an estimate from a two-dimensional displacement spectrum appearing in Sherman and Pinkel (1991). Further details and a regional characterization of these data appear in PL. Finally, power laws of a two-dimensional vertical wavenumber–frequency spectrum, $e(m,\omega) \propto \omega^{-c}m^{-d}$, correspond to the power laws of a three-dimensional vertical wavenumber–horizontal wavenumber action spectrum $n(k,m) \propto k^{-a}m^{-b}$ with the mapping,

$$a = c + 2 \quad \text{and} \quad b = d - c.$$

Figure 1 suggests that the data points are not randomly distributed but have some pattern. Explaining the location of the experimental points and making sense out of this pattern is the main physical motivation for this study.

c. Hamiltonian structure and wave turbulence theory

This subsection briefly summarizes the derivation in Lvov and Tabak (2001, 2004); it is included here only for completeness and to allow references from the core of the paper.

The equations of motion satisfied by an incompressible stratified rotating flow in hydrostatic balance under the Boussinesq approximation are (Cushman-Roisin 1994)

$$\begin{aligned} \frac{\partial}{\partial t}\frac{\partial z}{\partial \rho} + \nabla\cdot\left(\frac{\partial z}{\partial \rho}\mathbf{u}\right) &= 0,\\ \frac{\partial \mathbf{u}}{\partial t} + f\mathbf{u}^{\perp} + \mathbf{u}\cdot\nabla\mathbf{u} + \frac{\nabla M}{\rho_0} &= 0,\\ \frac{\partial M}{\partial \rho} - gz &= 0. \end{aligned} \tag{6}$$

These equations result from mass conservation, horizontal-momentum conservation, and hydrostatic balance. The

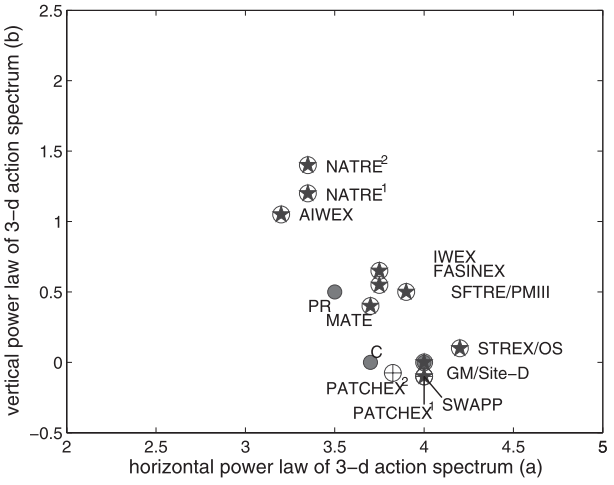

FIG. 1. The observational points. The filled circles represent the PR spectrum [$(a, b) = (3.5, 0.5)$], the convergent numerical solution determined in section 4c [$(a, b) = (3.7, 0.0)$], and the GM spectrum [$(a, b) = (4.0, 0.0)$]. Circles with stars represent estimates based on 1D spectra from the western North Atlantic south of the Gulf Stream (IWEX, FASINEX, and SFTRE/PMIII), the eastern North Pacific (STREX/OS and PATCHEX[1]), the western North Atlantic north of the Gulf Stream (Site-D), the Arctic (AIWEX), and the eastern North Atlantic (NATRE[1] and NATRE[2]). There are two estimates obtained from 2D datasets from the eastern North Pacific (SWAPP and PATCHEX[2]) represented as circles with crosshairs. NATRE[1] and NATRE[2] represent fits to the observed spectra and observed minus vortical mode spectra, respectively. Therefore NATRE[2] represents the best estimate of the NATRE internal-wave spectrum. To conclude, 12 observational points from 10 observational programs are shown (because 2 programs produced 2 points each). Note that PATCHEX[1] is indistinguishable from SWAPP. Also note that one of the three filled circles (GM) coincides with the experimental point from Site-D.

equations are written in isopycnal coordinates with the density ρ replacing the height z in its role as independent vertical variable. Here $\mathbf{u} = (u, v)$ is the horizontal component of the velocity field; $\mathbf{u}^\perp = (-v, u)$; $\nabla = (\partial/\partial x, \partial/\partial y)$ is the gradient operator along isopycnals; M is the Montgomery potential,

$$M = P + g\rho z;$$

f is the Coriolis parameter; and ρ_0 is a reference density in its role as inertia, considered constant under the Boussinesq approximation.

The potential vorticity is given by

$$q = \frac{f + (\partial v/\partial x) - (\partial u/\partial y)}{\Pi}, \tag{7}$$

where $\Pi = \rho/g\partial^2 M/\partial\rho^2 = \rho\partial z/\partial\rho$ is a normalized differential layer thickness. Because both the potential vorticity and the fluid density are conserved along particle trajectories, an initial profile of the potential vorticity that is a function of the density will be preserved by the flow. Hence, it is self-consistent to assume that

$$q(\rho) = q_0(\rho) = \frac{f}{\Pi_0(\rho)}, \tag{8}$$

where $\Pi_0(\rho) = -g/N(\rho)^2$ is a reference stratification profile with constant background buoyancy frequency, $N = (-g/(\rho\partial z/\partial\rho|_{\text{bg}}))^{1/2}$, independent of x and y. This assumption is not unrealistic: it represents a pancake-like distribution of potential vorticity, the result of its comparatively faster homogenization along than across isopycnal surfaces.

It is shown in Lvov and Tabak (2001, 2004) that the primitive equations of motion (6) under the assumption (8) can be written as a pair of canonical Hamiltonian equations,

$$\frac{\partial\Pi}{\partial t} = -\frac{\delta\mathcal{H}}{\delta\phi} \quad \text{and} \quad \frac{\partial\phi}{\partial t} = \frac{\delta\mathcal{H}}{\delta\Pi}, \tag{9}$$

where ϕ is the isopycnal velocity potential and the Hamiltonian is the sum of kinetic and potential energies,

$$\mathcal{H} = \int d\mathbf{x}\, d\rho \left\{ -\frac{1}{2}[\Pi_0 + \Pi(\mathbf{x},\rho)] \left| \nabla\phi(\mathbf{x},\rho) + \frac{f}{\Pi_0}\nabla^\perp\Delta^{-1}\Pi(\mathbf{x},\rho) \right|^2 + \frac{g}{2}\left| \int^\rho d\rho' \frac{\Pi(\mathbf{x},\rho')}{\rho'} \right|^2 \right\}. \tag{10}$$

Here, $\nabla^\perp = (-\partial/\partial y, \partial/\partial x)$, Δ^{-1} is the inverse Laplacian, and ρ' represents a variable of integration rather than perturbation.

Switching to Fourier space and introducing a complex field variable $c_{\mathbf{p}}$ through the transformation

$$\begin{aligned} \phi_{\mathbf{p}} &= \frac{iN\sqrt{\omega_{\mathbf{p}}}}{\sqrt{2g|\mathbf{k}|}}(c_{\mathbf{p}} - c^*_{-\mathbf{p}}), \\ \Pi_{\mathbf{p}} &= \Pi_0 - \frac{N\Pi_0|\mathbf{k}|}{\sqrt{2g\omega_{\mathbf{p}}}}(c_{\mathbf{p}} + c^*_{-\mathbf{p}}), \end{aligned} \tag{11}$$

where the frequency ω satisfies the linear dispersion relation[2]

$$\omega_{\mathbf{p}} = \sqrt{f^2 + \frac{g^2}{\rho_0^2 N^2}\frac{|\mathbf{k}|^2}{m^2}}, \tag{12}$$

the equations of motion (6) adopt the canonical form

$$i\frac{\partial}{\partial t}c_{\mathbf{p}} = \frac{\delta \mathcal{H}}{\delta c_{\mathbf{p}}^*}, \tag{13}$$

with Hamiltonian

$$\mathcal{H} = \int d\mathbf{p}\omega_{\mathbf{p}}|c_{\mathbf{p}}|^2 + \int d\mathbf{p}_{012}[\delta_{\mathbf{p}+\mathbf{p}_1+\mathbf{p}_2}(U_{\mathbf{p},\mathbf{p}_1,\mathbf{p}_2}c_{\mathbf{p}}^* c_{\mathbf{p}_1}^* c_{\mathbf{p}_2}^* + \text{c.c.}) + \delta_{-\mathbf{p}+\mathbf{p}_1+\mathbf{p}_2}(V_{\mathbf{p}_1,\mathbf{p}_2}^{\mathbf{p}} c_{\mathbf{p}}^* c_{\mathbf{p}_1} c_{\mathbf{p}_2} + \text{c.c.})]. \tag{14}$$

This is the standard form of the Hamiltonian of a system dominated by three-wave interactions (Zakharov et al. 1992). Calculations of interaction coefficients are tedious but straightforward tasks, completed in Lvov and Tabak (2001, 2004). These coefficients are given by

$$V_{\mathbf{p}_1,\mathbf{p}_2}^{\mathbf{p}} = \frac{N}{4\sqrt{2g}}\frac{1}{kk_1k_2}(I_{\mathbf{p},\mathbf{p}_1,\mathbf{p}_2} + J_{\mathbf{p}_1,\mathbf{p}_2}^{\mathbf{p}} + K_{\mathbf{p},\mathbf{p}_1,\mathbf{p}_2}), \tag{15a}$$

$$U_{\mathbf{p},\mathbf{p}_1,\mathbf{p}_2} = \frac{N}{4\sqrt{2g}}\frac{1}{3}\frac{1}{kk_1k_2}(I_{\mathbf{p},\mathbf{p}_1,\mathbf{p}_2} + J_{\mathbf{p}_1,\mathbf{p}_2}^{-\mathbf{p}} + K_{\mathbf{p},\mathbf{p}_1,\mathbf{p}_2}), \tag{15b}$$

$$I_{\mathbf{p},\mathbf{p}_1,\mathbf{p}_2} = -\sqrt{\frac{\omega_1\omega_2}{\omega}}k^2\mathbf{k}_1\cdot\mathbf{k}_2 - [(0,1,2)\to(1,2,0)] - [(0,1,2)\to(2,0,1)], \tag{15c}$$

$$J_{\mathbf{p}_1,\mathbf{p}_2}^{\mathbf{p}} = \frac{f^2}{\sqrt{\omega\omega_1\omega_2}}\{k^2\mathbf{k}_1\cdot\mathbf{k}_2 - [(0,1,2)\to(1,2,0)] - [(0,1,2)\to(2,0,1)]\}, \quad \text{and} \tag{15d}$$

$$K_{p,p_1p_2} = -if\left\{\sqrt{\frac{\omega}{\omega_1\omega_2}}(k_1^2 - k_2^2)\mathbf{k}_1\cdot\mathbf{k}_2^{\perp} + [(0,1,2)\to(1,2,0)] + [(0,1,2)\to(2,0,1)]\right\}, \tag{15e}$$

where $[(0,1,2)\to(1,2,0)]$ and $[(0,1,2)\to(2,0,1)]$ denote exchanges of suffixes and, for two dimensional vector $\mathbf{k} = (k_x, k_y)$, $\mathbf{k}^{\perp} = (-k_y, k_x)$.[3] We stress that the field Eq. (13) with the three-wave Hamiltonian [(12), (14), and (15)] is equivalent to the primitive equations of motion for internal waves (6). The approach using a Lagrangian coordinate system is based on small-amplitude expansion to arrive at this type of equation.

In wave turbulence theory, one proposes a perturbation expansion in the amplitude of the nonlinearity, yielding linear waves at the leading order. Wave amplitudes are modulated by the nonlinear interactions, and the modulation is statistically described by a kinetic equation (Zakharov et al. 1992) for the wave action $n_{\mathbf{p}}$ defined by

$$n_{\mathbf{p}}\delta(\mathbf{p}-\mathbf{p}') = \langle c_{\mathbf{p}}^* c_{\mathbf{p}'}\rangle. \tag{16}$$

Here $\langle\cdot\rangle$ denotes an ensemble averaging: that is, averaging over many realizations of the random wave field. The derivation of this kinetic equation is well studied and understood (Zakharov et al. 1992; Lvov and Nazarenko 2004). For the three-wave Hamiltonian (14), the kinetic equation is the one in Eq. (1), describing general internal waves interacting in both rotating and nonrotating environments.

The delta functions in the kinetic equation ensures that spectral transfer happens on the resonant manifold, which is defined as

$$\text{(a)}\begin{cases}\mathbf{p} = \mathbf{p}_1 + \mathbf{p}_2\\ \omega = \omega_1 + \omega_2\end{cases},\quad \text{(b)}\begin{cases}\mathbf{p}_1 = \mathbf{p}_2 + \mathbf{p}\\ \omega_1 = \omega_2 + \omega\end{cases},\quad \text{(c)}\begin{cases}\mathbf{p}_2 = \mathbf{p} + \mathbf{p}_1\\ \omega_2 = \omega + \omega_1\end{cases}. \tag{17}$$

Now let us assume that the wave action n is independent of the direction of the horizontal wavenumber and is symmetric with respect to $m \to -m$ change,

$$n_{\mathbf{p}} = n(|\mathbf{k}|, |m|).$$

Note that value of the interaction matrix element is independent of horizontal azimuth because it depends only on the magnitude of interacting wavenumbers. Therefore, one can integrate the kinetic Eq. (1) over horizontal azimuth (Zakharov et al. 1992), yielding

[2] This dispersion relation is written in the isopycnal framework. In the more familiar Eulerian framework, the dispersion relation transforms into $\omega_{\mathbf{p}} = \sqrt{f^2 + (N^2k^2/m_*^2)}$, where m_*, the vertical wavenumber in z coordinates, is given by $m_* = -(g/\rho_0 N^2)m$.

[3] We note that these are correct expressions, which coincide with those given in Lvov and Tabak (2004), apart from a few ½ factors.

$$\frac{\partial n_{\mathbf{p}}}{\partial t} = \frac{2}{k}\int (R^0_{12} - R^1_{20} - R^2_{01})\, dk_1\, dk_2\, dm_1\, dm_2,$$
$$R^0_{12} = f^{\mathbf{p}}_{\mathbf{p}_1\mathbf{p}_2} |V^{\mathbf{p}}_{\mathbf{p}_1\mathbf{p}_2}|^2 \delta_{m-m_1-m_2}\delta_{\omega_{\mathbf{p}}-\omega_{\mathbf{p}_1}-\omega_{\mathbf{p}_2}} kk_1k_2/S^0_{1,2}. \quad (18)$$

Here, $S^0_{1,2}$ appears as the result of integration of the horizontal-momentum conservative delta function over all possible orientations and is equal to the area of the triangle with sides with the length of the horizontal wavenumbers $k = |\mathbf{k}|$, $k_1 = |\mathbf{k}_1|$ and $k_2 = |\mathbf{k}_2|$. This is the form of the kinetic equation that will be used to find scale-invariant solutions in the next section.

3. Scale-invariant kinetic equation

a. Reduction of kinetic equation to the resonant manifold

In the high-frequency limit $\omega \gg f$, one could conceivably neglect the effects of the rotation of the earth. The dispersion relation (12) then becomes (Lvov and Tabak 2001)

$$\omega_{\mathbf{p}} \equiv \omega_{\mathbf{k},m} \simeq \frac{g}{\rho_0 N}\frac{|\mathbf{k}|}{|m|}, \quad (19)$$

and, in this limit, the matrix element (15) retains only its first term, $I_{\mathbf{p},\mathbf{p}_1,\mathbf{p}_2}$.

The azimuthally integrated kinetic Eq. (18) includes integration over k_1 and k_2, because the integrations over m_1 and m_2 can be done by using delta functions. To use delta functions, we need to perform what is called reduction to the resonant manifold. Consider, for example, resonances of type (17a). Given k, k_1, k_2, and m, one can find m_1 and m_2 satisfying the resonant condition by solving simultaneous equations

$$m = m_1 + m_2 \quad \text{and} \quad \frac{k}{|m|} = \frac{k_1}{|m_1|} + \frac{k_2}{|m - m_1|}. \quad (20)$$

The solutions of this quadratic equation are given by

$$\begin{cases} m_1 = \dfrac{m}{2k}\left[k + k_1 + k_2 + \sqrt{(k + k_1 + k_2)^2 - 4kk_1}\right] \\ m_2 = m - m_1 \end{cases} \quad \text{and} \quad (21a)$$

$$\begin{cases} m_1 = \dfrac{m}{2k}\left[k - k_1 - k_2 - \sqrt{(k - k_1 - k_2)^2 + 4kk_1}\right]. \\ m_2 = m - m_1 \end{cases} \quad (21b)$$

Note that Eq. (21a) translates into Eq. (21b) if the indices 1 and 2 are exchanged. Indeed, exchanging indices 1 and 2 in Eq. (21a) we obtain

$$m_1' = m - m_2' = m - \frac{m}{2k}\left[k + k_1 + k_2 + \sqrt{(k + k_1 + k_2)^2 - 4kk_2}\right],$$

which simplifies then to m_1 of Eq. (21b).

Similarly, resonances of type (17b) yield

$$\begin{cases} m_2 = -\dfrac{m}{2k}\left[k - k_1 - k_2 + \sqrt{(k - k_1 - k_2)^2 + 4kk_2}\right] \\ m_1 = m + m_2 \end{cases} \quad \text{and} \quad (22a)$$

$$\begin{cases} m_2 = -\dfrac{m}{2k}\left[k + k_1 - k_2 + \sqrt{(k + k_1 - k_2)^2 + 4kk_2}\right], \\ m_1 = m + m_2 \end{cases} \quad (22b)$$

and resonances of type (17c) yield

$$\begin{cases} m_1 = -\dfrac{m}{2k}\left[k - k_1 - k_2 + \sqrt{(k - k_1 - k_2)^2 + 4kk_1}\right] \\ m_2 = m + m_1 \end{cases} \quad \text{and} \quad (23a)$$

$$\begin{cases} m_1 = -\dfrac{m}{2k}\left[k - k_1 + k_2 + \sqrt{(k - k_1 + k_2)^2 + 4kk_1}\right]. \\ m_2 = m + m_1 \end{cases} \quad (23b)$$

After this reduction, a double integral over k_1 and k_2 is left. The domain of integration is further restricted by the triangle inequalities

$$k < k_1 + k_2, \quad k_1 < k + k_2, \quad \text{and} \quad k_2 < k + k_1. \quad (24)$$

These conditions ensure that one can construct a triangle out of the wavenumbers with lengths k, k_1, and k_2 and determine the domain in the (k_1, k_2) plane called the kinematic box in the oceanographic literature.

Numerical evaluation of the collision integral is a complicated but straightforward task. Interpretation of the results, though, is more difficult, mostly because of the complexity of the interaction matrix element and the nontrivial nature of the resonant set. Starting with McComas and Bretherton (1977), therefore, predictions were made based on a further simplification. This simplification is based on the assertion that interactions between wavenumbers with extreme scale separation contribute mostly to the nonlinear dynamics. Three main classes of such resonant triads appear, characterized by extreme scale separation. These three main classes are as follows:

- The vertical backscattering of a high-frequency wave by a low-frequency wave of twice the vertical wavenumber into a second high-frequency wave of oppositely signed vertical wavenumber: this type of scattering, as in Eqs. (25a), (27b), (29a), and (30a) below, is called elastic scattering (ES).
- The scattering of a high-frequency wave by a low-frequency, small-wavenumber wave into a second, nearly identical, high-frequency, large-wavenumber wave: this type of scattering, as in Eqs. (25b), (27a), (29b), and (30b) below, is called induced diffusion.
- The decay of a small-wavenumber wave into two large-vertical-wavenumber waves of approximately one-half the frequency: this type of scattering, as in Eqs. (26a), (26b), (28a), (28b) below, is called parametric subharmonic instability (PSI).

To see how this classification appears analytically, we perform the limit of $k_1 \to 0$ and the limit $k_1 \to \infty$ in Eqs. (21)–(23). We will refer to the k_1 or $k_2 \to 0$ limits as IR limits, whereas the k_1 and $k_2 \to \infty$ limit will be referred as a UV limit. Because the integrals in the kinetic equation for power-law solutions will be dominated by the scale-separated interaction, this will help us analyze possible solutions to the kinetic equation.

The results of the $k_1 \to 0$ limit of Eqs. (21)–(23) are given by

$$\begin{cases} m_1 \to 2m, & m_2 \to -m \\ \omega_1 \ll \omega, & \omega_2 \sim \omega \end{cases}, \tag{25a}$$

$$\begin{cases} -m_1 \ll m, & m_2 \sim m \\ \omega_1 \ll \omega, & \omega_2 \sim \omega \end{cases}, \tag{25b}$$

$$\begin{cases} m_1 \ll m, & m_2 \sim -m \\ \omega_1 \sim 2\omega, & \omega_2 \sim \omega \end{cases}, \tag{26a}$$

$$\begin{cases} -m_1 \ll m, & m_2 \sim -m \\ \omega_1 \sim 2\omega, & \omega_2 \sim \omega \end{cases}, \tag{26b}$$

$$\begin{cases} -m_1 \ll m, & m_2 \sim m \\ \omega_1 \ll \omega, & \omega_2 \sim \omega \end{cases}, \quad \text{and} \tag{27a}$$

$$\begin{cases} m_1 \to -2m, & m_2 \to -m \\ \omega_1 \ll \omega, & \omega_2 \sim \omega \end{cases}. \tag{27b}$$

We now see that the interactions (25a) and (27b) correspond to the ES mechanism, that the interactions (25b) and (27a) correspond to the ID, and that the interactions (26a) and (26b) correspond to the PSI.

Similarly, taking the k_1 and $k_2 \to \infty$ limits of Eqs. (21)–(23), we obtain

$$\begin{cases} m_1 \gg m, & -m_2 \gg m \\ \omega_1, \omega_2 \sim \omega/2 \end{cases}, \tag{28a}$$

$$\begin{cases} -m_1 \gg m, & m_2 \gg m \\ \omega_1, \omega_2 \sim \omega/2 \end{cases}, \tag{28b}$$

$$\begin{cases} m_1 \sim m/2, & m_2 \sim -m/2 \\ \omega_1, \omega_2 \gg \omega \end{cases}, \tag{29a}$$

$$\begin{cases} -m_1 \gg m, & -m_2 \gg m \\ \omega_1, \omega_2 \gg \omega \end{cases}, \tag{29b}$$

$$\begin{cases} m_1 \sim -m/2, & m_2 \sim m/2 \\ \omega_1, \omega_2 \gg \omega \end{cases}, \quad \text{and} \tag{30a}$$

$$\begin{cases} -m_1 \gg m, & -m_2 \gg m \\ \omega_1, \omega_2 \gg \omega \end{cases}. \tag{30b}$$

We now can identify the interactions (28a) and (28b) as being PSI, the interactions (29a) and (30a) as being ES, and the interactions (29b) and (30b) as being ID.

This classification provides an easy and intuitive tool for describing extremely scale-separated interactions. We will see below that one of these interactions, namely ID, explains reasonably well the experimental data that is available to us.

b. Convergences and divergences of the kinetic equation

Neglecting the effects of the rotation of the earth yields a scale-invariant system with dispersion relation given by Eq. (19) and matrix element given only by the $I_{\mathbf{p},\mathbf{p}_1,\mathbf{p}_2}$ in Eq. (15). This is the kinetic equation of Lvov and Tabak (2001), Lvov et al. (2004), and Lvov and Tabak (2004), describing internal waves in hydrostatic balance in a nonrotating environment.

Proposing a self-similar separable spectrum of the form (2), one can show from the azimuthally integrated kinetic Eq. (18) that (Zakharov et al. 1992)

$$\frac{\partial n(\alpha\mathbf{k}, \beta m)}{\partial t} = \alpha^{4-2a}\beta^{1-2b}\frac{\partial n(\mathbf{k}, m)}{\partial t} \tag{31}$$

for constants α and β. To find a steady scale-invariant solution for all values of k and m, it is therefore sufficient to find exponents that give a 0 collision integral for one wavenumber. One can fix k and m, adopting for instance $k = m = 1$, and seek 0 of the collision integral (represented as $\mathcal{C}$ below) as a function of a and b,

$$\frac{\partial n(k=1, m=1)}{\partial t} \equiv \mathcal{C}(a, b). \tag{32}$$

Before embarking on numerical or analytical integration of the kinetic Eq. (18) with scale-invariant solutions (2), it is necessary to check whether the collision integral converges. Appendix A outlines these calculations. The condition for the scale-invariant collision integral (32) to converge at the IR end, k_1 or $k_2 \to 0$, is given by

$$a + b/2 - 7/2 < 0 \quad \text{and} \quad -3 < b < 3, \tag{33a}$$

$$a - 4 < 0 \quad \text{and} \quad b = 0, \tag{33b}$$

$$a - 7/2 < 0 \quad \text{and} \quad b = 1, \tag{33c}$$

$$a + b - 5 < 0 \quad \text{and} \quad b > 3, \quad \text{or} \tag{33d}$$

$$a - 5 < 0 \quad \text{and} \quad b < -3. \tag{33e}$$

Similarly, UV convergence as k_1 and $k_2 \to \infty$ implies that

$$a + b/2 - 4 > 0 \quad \text{and} \quad -2 < b < 2, \tag{34a}$$

$$a - 7/2 > 0 \quad \text{and} \quad b = 0, \tag{34b}$$

$$a - 3 > 0 \quad \text{and} \quad b > 2, \quad \text{or} \tag{34c}$$

$$a + b - 3 > 0 \quad \text{and} \quad b < -2. \tag{34d}$$

The domains of divergence and convergence are shown in Fig. 2.

Figure 2 also displays the classes of triads dominating the interactions. Knowing the classes of interactions that lead to the divergences of the kinetic equation allows us to find possible physical scenarios of the convergent solutions or to find a possible physical regularization of the divergences.

Note that, in addition to the two-dimensional domain of IR convergence [the regions (33a), (33d), and (33e)], there are two additional IR convergent line segments given by Eqs. (33b) and (33c). These two special line segments appear because of the $b(b - 1)$ prefactor to the divergent contributions to the collision integral (A3). Similarly, for the UV limit, in addition to the two-dimensional region of convergence [(33a), (34c), and (34d)], there is an additional special line segment of $b = 0$ [(34b)].

We see that these domains of convergence overlap only on the segment

$$7/2 < a < 4 \quad \text{and} \quad b = 0. \tag{35}$$

This result contradicts the one in Lvov et al. (2004), where a coding error led us to believe that the integrals converge and that GM is an exact steady-state solution to the scale-invariant kinetic equation. Note that $b = 0$ corresponds to wave action independent of vertical wavenumbers, $\partial n/\partial m = 0$. Existence of the $b = 0$ line will allow us to find novel convergent solution in section 4. We also note that the IR segment on $b = 0$ coincides with one of the ID solutions determined in section 6. The other segment on $b = 1$ does not coincide with the ID solution in section 6, because the scale-invariant system has higher symmetry than the system with Coriolis effect.

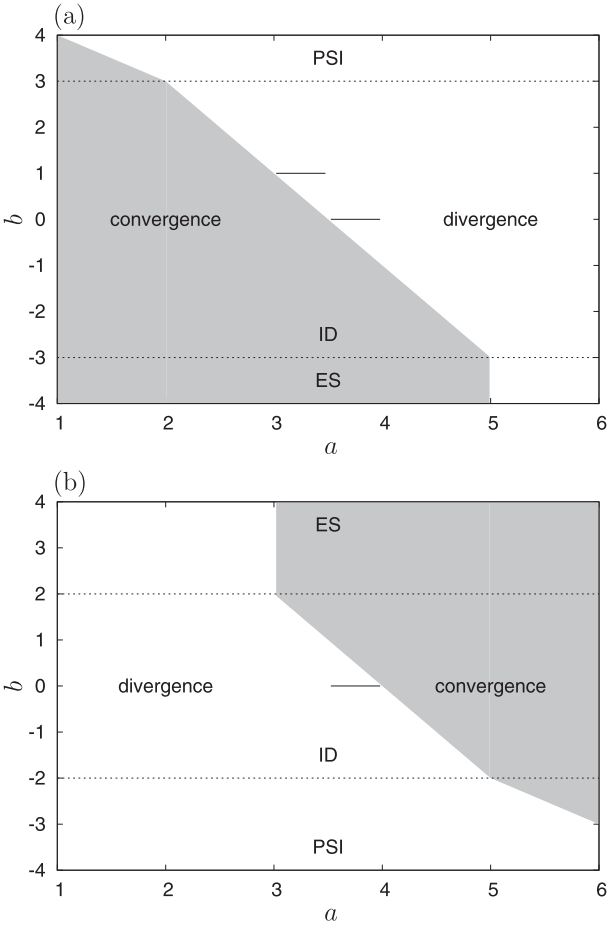

FIG. 2. (a) Convergence and (b) divergence due to (a) IR wavenumbers and (b) UV wavenumbers. The integral converge for the exponents in the shaded regions or on the segments ($b = 0, 7/2 < a < 4$) and ($b = 1, 3 < a < 7/2$). Dashed lines distinguish the domains where the indicated named triads dominate the singularity.

4. A novel convergent solution

To find out whether there is a steady solution of the kinetic equation along the convergent segment (35), we substitute the power-law ansatz (2) with $b = 0$ into the azimuthally integrated kinetic Eq. (18). We then compute numerically the collision integral as a function of a for $b = 0$. To this end, we fix $k = m = 1$ and perform a numerical integration over the kinematic box (24),

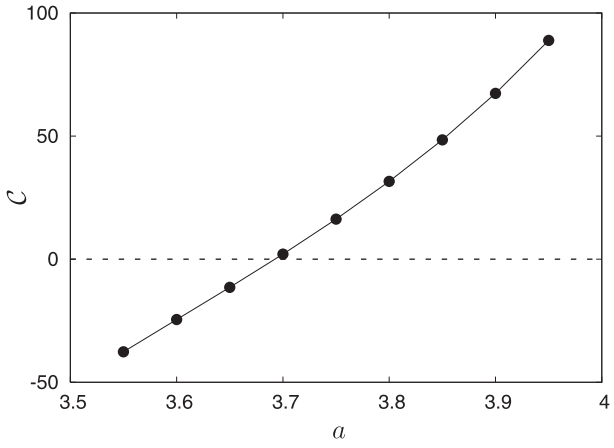

FIG. 3. Value of the collision integral as a function of a on the convergent segment, $b = 0$.

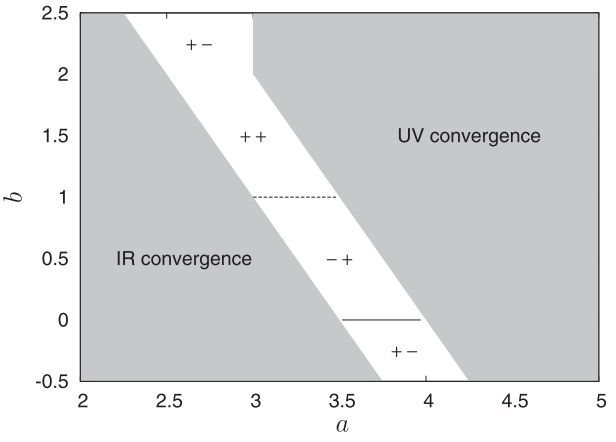

FIG. 4. Signs of the divergences where the both IR and UV contributions diverge. The left symbols show the signs due to IR wavenumbers and the right symbols show the signs due to UV wavenumbers.

reducing the integral to the resonant manifold as described in section 3a.

The result of this numerical integration is shown in Fig. 3. The figure clearly shows the existence of a steady solution of the kinetic Eq. (18) near $a \cong 3.7$ and $b = 0$.

This is, therefore, the only convergent steady solution to the scale-invariant kinetic equation for the internal-wave field. It is highly suggestive that it should exist so close to the GM spectrum, $a = 4$ and $b = 0$ for large wavenumbers, the most agreed upon fit to the spectra observed throughout the ocean. It remains to be seen whether and how this solution is modified by inclusion of background rotation.

5. Balance between divergences

The fact that the collision integral $\mathcal{C}$ diverges for almost all values of a and b can be viewed both as a challenge and as a blessing. On one hand, it makes the prediction of steady spectral slopes more difficult, because it now depends on the details of the truncation of the domain of the integration. Fortunately, it provides a powerful tool for quantifying the effects of fundamental players in ocean dynamics, most of which live on the fringes of the inertial subrange of the internal-wave field: the Coriolis effect, as well as tides and storms, at the IR end of the spectrum and wave breaking and dissipation at the UV end. The sensitive response of the inertial subrange to the detailed modeling of these scale-separated mechanisms permits, in principle, building simple models in which these are the only players, bypassing the need to consider the long range of wave scales in between.

At the IR end, the resonant interactions are dominated by the ID singularity for $-3 < b < 3$ (Fig. 2). The sign of the divergences is given by $-b(b-1)$ [Eq. (A3)]. Similarly, at the UV end, resonant interactions are dominated by the ID singularity for $-2 < b < 2$ (Fig. 2). The sign of the divergence is given by b [Eq. (A4)]. At the UV end for $b > 2$, where ES determines the divergences, the sign of the singularity is given by $-b$: that is, the sign is negative [Eq. (A5)]. Figure 4 shows the signs of the divergences where both the IR and UV contributions diverge: the left sign corresponds to the IR contribution, and the right sign corresponds to the UV contribution.

Hence, in the regions,

$$7 < 2a + b < 8 \quad \text{and} \quad -2 < b < 1 \quad \text{or} \qquad \text{(36a)}$$

$$7 < 2a + b, \quad a < 3, \quad \text{and} \quad b > 2, \qquad \text{(36b)}$$

the divergences of the collision integral at the IR and UV ends have opposite signs. Then formal solutions can be constructed by having these two divergences cancel each other out.

This observation justifies the existence of the PR solution (5). Indeed, the PR spectrum has divergent power-law exponents at the both ends. One can prove that the PR spectrum is an exact steady solution of the kinetic Eq. (1) by applying the Zakharov–Kuznetsov conformal mapping for systems with cylindrical symmetry (Zakharov 1968, 1967; Kuznetsov 1972). This Zakharov–Kuznetsov conformal mapping effectively establishes a map between the neighborhoods of zero and infinity. Making these two contributions cancel pointwise yields the solution (5). For this transformation to be mathematically applicable, the integrals have to converge. This transformation leads only to a formal solution for divergent integrals. Some other transformation, as we explain below, may lead to completely different solutions.

The PR spectrum was first found by Pelinovsky and Raevsky (1977). However, they realized that it was only a formal solution. The solution was found again in Caillol and Zeitlin (2000) through a renormalization argument and in Lvov and Tabak (2001, 2004) within an isopycnal formulation of the wave field.

The idea of a formal solution, such as PR, can be generalized quite widely: in fact, any point in the regions with opposite-signed divergences can be made into a steady solution under a suitable conformal mapping that makes the divergences at zero and infinity cancel each other, as does the Zakharov–Kuznetsov transformation. Such generalized Zakharov–Kuznetsov transformation is an extension of the idea of principal value for a divergent integral, whereby two divergent contributions are made to cancel each other through a specific relation between their respective contributions.

Indeed, in the ocean internal waves cannot have zero horizontal wavenumber. Rather, a smallest horizontal wavenumber exists, which corresponds to largest horizontal scales of internal waves. The largest wavenumber that was observed is on the order of thousands of kilometers. On larger scales, β effects become important, and they prevent wavenumbers to achieve even smaller scales. Other effects possibly affecting small wavenumbers include ocean storms, interactions with large scale vortices and shear, and ocean boundaries. Similarly, there is no infinitely large wavenumber for internal waves, but rather there is possibly large horizontal wavenumber that is affected by wave breaking, interaction with the turbulence, and other processes.

The idea of a generalized Zakharov–Kuznetsov transformation leading to an infinite number of steady states provides a possible explanation for the variability of the power-law exponents of the quasi-steady spectra: inertial subrange spectral variability is to be expected when it is driven by the nonlocal interactions. The natural local variability of players outside the inertial range translates into a certain degree of nonuniversality. Such players include storms and tides, as well as possible geometrical constrains and interactions with large-scale shear and vortices. Investigation of the nature of possible balances between IR and UV divergences is outside of scope of the present paper.

6. Regularization by the Coriolis effect

Physically, the ocean does not perform generalized Zakharov–Kuznetsov transformation. However, in the ocean there are finite boundaries in the frequency domain. In particular, the inertial frequency f provides a truncation for the IR part of the spectrum, whereas the UV truncation is provided by the buoyancy frequency N. These two frequencies vary from place to place, giving grounds for spectral variability. Consequently, the integrals are not truly divergent, but rather they have a large numerical value dictated by the location of the IR cutoff.

Note that the $f \to 0$ calculations presented in this section describe intermediate frequencies ω such that $\omega \gg f > 0$. Consequently, these intermediate frequencies feel inertial frequency as being small. These calculations will not be applicable for equatorial regions, where f is identically zero.

Observe that all the experimental points are located in regions of the (a, b) domain $a > (-b + 7)/2$ for which the integral diverges in the IR region. Also note that 5 out of 12 experimental points are located in the region where collision integrals are UV convergent: that is, in $a > -b/2 + 4$. The UV region is therefore assumed to be either subdominant or convergent in this section, where we study the regularization resulting from a finite value of f.

We note that, because we consider scale-invariant case only in the present paper, the IR cutoff can equivalently be considered as k approaching smallest possible value or equivalently when ω approaches its smallest value. Because the IR cutoff is given by f, a frequency, it is easier to analyze the resulting integral in (ω_1, m_1) rather than in the more traditional (k_1, m_1) domain utilized in Müller et al. (1986) and the previous sections. We emphasize that the present paper concerns itself with scale-invariant wave action spectrum (2). The scale-invariant wave action can be translated from (k_1, m_1) to (ω_1, m_1) domain with out loss of generality. This statement would not be true for the realistic Garrett–Munk spectrum or any other oceanic spectrum because of the non-scale-invariant form of the linear dispersion relation (12). Such spectra will be analyzed in subsequent publication (LPY).

Therefore, to proceed, we assume a power-law spectrum, similar to Eq. (2), but in the (ω, m) space,

$$n_{\omega,m} \propto \omega^{\tilde{a}} m^{\tilde{b}}. \tag{37}$$

We need to transform the wave action as a function of k and m to a function of ω and m. This is done in appendix B. The relation between a, b and $\tilde{a}, \tilde{b}$ reads as

$$\tilde{a} = -a, \quad \tilde{b} = -a - b.$$

Thus, we need to express both the kinetic equation and the kinematic box in terms of frequency and vertical wavenumber. For this, we use the dispersion relation

(12) to express k in terms of ω in the description of the kinematic box (24),

$$\omega_1 < E_3(m_1), \quad \omega_1 > E_4(m_1), \quad \omega_1 > E_1(m_1) \quad \text{if} \quad m_1 < 0, \quad \omega_1 > \omega; \tag{38a}$$

$$\omega_1 > E_3(m_1), \quad \omega_1 < E_4(m_1), \quad \omega_1 < E_1(m_1) \quad \text{if} \quad m_1 < 0, \quad \omega_1 < \omega; \tag{38b}$$

$$\omega_1 < E_2(m_1), \quad \omega_1 > E_2(m_1), \quad \omega_1 > E_4(m_1) \quad \text{if} \quad m_1 > 0, \quad \omega_1 < \omega; \quad \text{and} \tag{38c}$$

$$\omega_1 > E_3(m_1), \quad \omega_1 < E_1(m_1), \quad \omega_1 < E_2(m_1) \quad \text{if} \quad m_1 > 0, \quad \omega_1 > \omega, \tag{38d}$$

where we have introduced the four curves in the (ω_1, m_1) domain that parameterize the kinematic box,

$$E_1(\omega_1) = m\frac{-\sqrt{-f^2+\omega^2}+\sqrt{-f^2+(\omega-\omega_1)^2}}{\sqrt{-f^2+\omega_1^2}+\sqrt{-f^2+(\omega-\omega_1)^2}},$$

$$E_2(\omega_1) = m\frac{\sqrt{-f^2+\omega^2}+\sqrt{-f^2+(\omega-\omega_1)^2}}{\sqrt{-f^2+\omega_1^2}+\sqrt{-f^2+(\omega-\omega_1)^2}},$$

$$E_3(\omega_1) = m\frac{-\sqrt{-f^2+\omega^2}+\sqrt{-f^2+(\omega-\omega_1)^2}}{-\sqrt{-f^2+\omega_1^2}+\sqrt{-f^2+(\omega-\omega_1)^2}}, \quad \text{and}$$

$$E_4(\omega_1) = m\frac{\sqrt{-f^2+\omega^2}+\sqrt{-f^2+(\omega-\omega_1)^2}}{-\sqrt{-f^2+\omega_1^2}+\sqrt{-f^2+(\omega-\omega_1)^2}}.$$

The kinematic box in the (ω, m) domain is shown in Fig. 5. Note that the region (38b) and (38c) can be transferred to each other by interchanging indices 1 and 2; consequently, two disconnected $\omega_1 < \omega$ regions look like mirrored and shifted copies of each other. To help in the transition from the traditional kinematic box (24) to the kinematic box in (ω, m) domain, the following limits were identified:

- ID1 is the ID limit of Eq. (25b) with indices 1 and 2 being flipped;

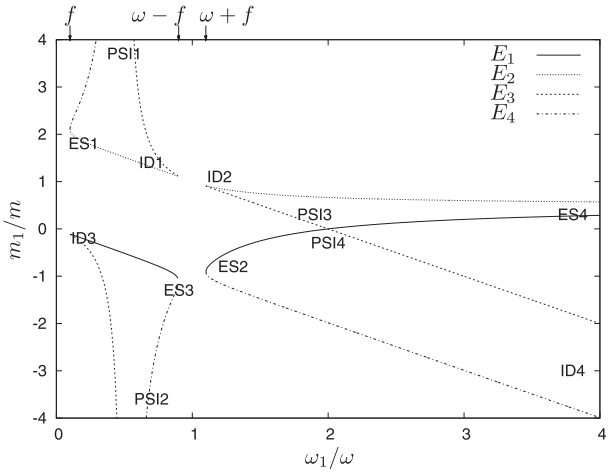

FIG. 5. The kinematic box in the (ω_1, m_1) domain. Two disconnected regions where $\omega_1 < \omega$ depict regions with "sum" interactions: namely, $\omega = \omega_1 + \omega_2$ and $m = m_1 + m_2$ types of the resonances. The connected regions where $\omega_1 > \omega$ depict "difference" resonances, $\omega_2 = \omega_1 - \omega$ and $m_2 = m_1 - m$. The parameters are chosen so that $f/\omega = 0.1$. Frequency f is marked on the top of the graph, and frequency N is outside of the region of frequencies shown on the graph.

- ID2 is the ID limit of Eq. (27a) with indices 1 and 2 being flipped;
- ID3 is the ID limit of Eq. (25b);
- ID4 is the ID limit of Eqs. (29b) and (30b);
- PSI1 is the PSI limit of Eq. (28a);
- PSI2 is the PSI limit of Eq. (28b);
- PSI3 is the PSI limit of Eq. (26a);
- PSI4 is the PSI limit of Eq. (26b);
- ES1 is the ES limit of Eq. (25a);
- ES2 is the ES limit of Eq. (27b) with indices 1 and 2 being flipped;
- ES3 is the ES limit of Eq. (27b) with indices 1 and 2 being flipped; and
- ES4 is the ES limit of Eq. (29a).

An advantage of the (ω, m) presentation for the kinematic box is that it allows a transparent reduction to the resonant manifold. A disadvantage is the curvilinear boundaries of the box, which requires more sophisticated analytical treatment.

Equation (18) transforms into

$$\frac{\partial}{\partial t}n[k(\omega,m),m] = \frac{1}{k}\int d\omega_1\, dm_1 J \frac{\left|V^0_{12}\right|^2}{S^0_{1,2}}[n_1 n_2 - n(n_1+n_2)]\big|_{\omega_2=\omega-\omega_1, m_2=m-m_1} - \frac{2}{k}\int d\omega_1\, dm_1 J \frac{\left|V^1_{02}\right|^2}{S^1_{2,0}} \times [nn_2 - n_1(n+n_2)]\big|_{\omega_2=\omega_1-\omega, m_2=m_1-m}. \tag{39}$$

We have used the dispersion relation $k_i = m_i\sqrt{\omega_i^2 - f^2}$ and defined J as the Jacobian of the transformation from (k_1, k_2) into (ω_1, ω_2) times the kk_1k_2 factor,

$$J = kk_1k_2 \frac{dk_1}{d\omega_1}\frac{dk_2}{d\omega_2}.$$

In Fig. 5, there are three ID regions (or corners) with significant contribution to the collision integral in the IR limit:

1) ID1 region: In this region, m_1 is slightly bigger than m, ω_1 is slightly smaller than ω, and ω_2 and m_2 are both very small. This region can be obtained from the region (38b) above by interchanging indices 1 and 2. In this region, the wave action n_2 is much smaller than wave action n and n_1:

$$n_2 \gg n, n_1.$$

2) ID2 region: In this region, ω_1 is slightly bigger than $\omega + f$, where $\omega_2 = \omega_1 - \omega$ is small and $m_2 = m_1 - m$ is negative and small. This is the region (38d). Also,

$$n_2 \gg n, n_1.$$

3) ID3 region: In this region, ω_1 is small and m_1 is small and negative. This corresponds to the region (38b), where wave action obeys

$$n_1 \gg n, n_2.$$

Note that this region can be obtained from the region ID1 by flipping indices 1 and 2. Consequently, only one of the ID1 and ID3 should be taken into account, with a factor of 2 multiplying the respective contribution. This also can be seen from Fig. 5 as ID1 and ID3 regions are shifted mirror images of each other.

Making these simplifications and taking into account the areas of integration in the kinematic box, we obtain

$$\frac{\partial}{\partial t}n[k(\omega,m),m] = \frac{2}{k}\int_f^{f+\omega_s}\int_{E_3(\omega_1)}^{E_1(\omega_1)} dm_1 J \frac{|V^0_{1,2}|^2}{S^0_{1,2}} n_1(n_2 - n)\, d\omega_1 - \frac{2}{k}\int_{\omega-f-\omega_s}^{\omega-f} d\omega_1 \int_{E_3(\omega_1)}^{E_1(\omega_1)} dm_1 J \frac{|V^2_{1,0}|^2}{S^2_{1,0}} n_2(n - n_1) \tag{40}$$

where the small parameter ω_s is introduced to restrict the integration to a neighborhood of the ID corners. The arbitrariness of the small parameter will not affect the end result below.

To quantify the contribution of near-inertial waves to a (ω, m) mode, we write

$$\epsilon \sim f \ll \omega = 1.$$

Subsequently, near the region ID3 of the kinematic box, we write

$$\omega_1 = f + \epsilon,$$

whereas near the ID2 corners of the kinematic box we write

$$\omega_1 = \omega + f + \epsilon.$$

We then expand the resulting analytical expression (40) in powers of ϵ and f without making any assumptions on their relative sizes. These calculations, including the integration over vertical wavenumbers m_1, are presented in appendix C. The resulting expression for the kinetic equation is given by

$$\frac{\partial}{\partial t}n[k(\omega,m),m] = \frac{\pi}{4k}(\tilde a - \tilde b)[\tilde a - 3(3+\tilde b)] \times m^{5+2\tilde b}\omega^{-3+\tilde a-\tilde b}\int_0^{\mu} d\epsilon(\epsilon + f)^{4+\tilde a+\tilde b}(\epsilon^2 + 2\epsilon f + 17f^2). \tag{41}$$

The integral over ϵ diverges at $\epsilon = 0$, if $f = 0$ and if $6 + \tilde a + \tilde b > -1$.[4]

However, if we postpone taking $f = 0$ limit, we see that the integral is 0 to leading order if

$$\tilde a - 3(3+\tilde b) = 0 \quad \text{or} \quad \tilde a - \tilde b = 0 \tag{42}$$

or, in terms of a and b,

$$9 - 2a - 3b = 0 \quad \text{or} \quad b = 0. \tag{43}$$

This is the family of power-law steady-state solutions to the kinetic equations dominated by infrared ID interactions. These steady states are identical to the ID stationary states identified by McComas and Bretherton (1977), who derived a diffusive approximation to their collision integral in the infrared ID limit. Note that

[4] Naturally, this condition coincides with (33a).

McComas and Müller (1981) interpreted $b = 0$ as a no-action flux in vertical wavenumber domain, whereas $9 - 2a - 3b = 0$ is a constant action flux solution.

We note that one can use the eikonal approach to describe these types of interactions (Flatté et al. 1985; Broutman et al. 2004; Müller et al. 1986; Henyey et al. 1986). An advantage of the eikonal approach versus our scale-invariant analysis is that it allows us to consider not only scale-invariant interactions in separable spectrum. The possible disadvantage of the eikonal approach is that construction of a transport theory is far less rigorous. For a more detailed discussion on the differences between the resonant interaction approximation and the eikonal approach, we refer the reader to Polzin (2004).

What is presented in this section is a rigorous asymptotic derivation of Eq. (43). These ID solutions help us to interpret observational data of Fig. 1 that are currently available to us. The value added associated with a rigorous asymptotic derivation is the demonstration that the ID stationary states are meaningful only in the IR divergent part of the (a, b) domain.

7. Conclusions

The results in this paper provide an interpretation of the variability in the observed spectral power laws. Combining Figs. 1, 2, and 4 with Eqs. (4), (5), and (43) produces the results shown in Fig. 6.

A nonrotating scale-invariant analysis provides two subdomains in which the kinetic equation converges in either the UV or the IR limit (light gray shading), two subdomains in which the kinetic equation diverges in both UV and IR limits but with oppositely signed values (dark gray shading) and a single domain with similarly signed UV and IR divergences (black shading). In this nonrotating analysis, a stationary state is possible only for oppositely signed divergences: that is, within the dark gray shaded regions. Six of the observational points lie in IR and UV divergent subdomains, and a seventh (Site-D) is on the boundary with the IR divergent–UV convergent subdomain. Two of the observational points lie in the domain of IR and UV divergence having similar signs, which does not represent a possible solution in the nonrotating analysis. These two points lie close to the boundaries of the ''forbidden'' (black shaded) region, and subtracting the vortical contribution from one (NATRE^1) returns a ''best'' estimate of the internal-wave spectrum (NATRE^2) that lies outside of the forbidden region.

All the data lie in an IR divergent regime and hence a regularization of the kinetic equation is performed by including a finite lower frequency of f. This produces a family of stationary states, the induced diffusion stationary states. These stationary states collapse much of the observed variability. The exception is the NATRE spectrum.

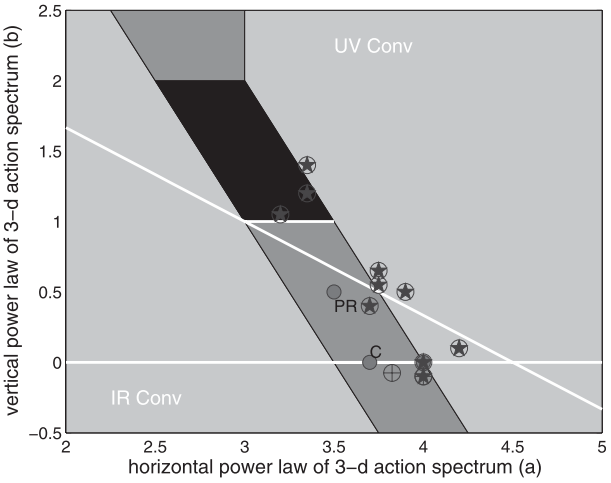

FIG. 6. The observational points and the theories: The filled circles represent the PR spectrum, the convergent numerical solution determined in section 4c, and the GM spectrum. Circles with stars represent power-law estimates based on 1D spectra. Circles with crosshairs represent estimates based on 2D datasets. See Fig. 1 for the identification of the field programs. Light gray shading represents regions of the power-law domain for which the collision integral converges in either the IR or UV limit. The dark gray shading represents the region of the power-law domain for which the IR and UV limits diverge and have opposite signs. The region of black shading represents the subdomain for which both the IR and UV divergences have the same sign: that is, when large contributions from interactions with very small and very large wavenumbers have the same sign. Overlaid as solid white lines are the ID stationary states.

Summarizing the paper, we have analyzed the scale-invariant kinetic equation for internal gravity waves and shown that its collision integral diverges for almost all spectral exponents. Figure 6 shows that the integral nearly always diverges at zero, at infinity, or at both ends. This means that, in the wave turbulence kinetic equation framework, the energy transfer is dominated by the scale-separated interactions with large and/or small scales.

The only exception where the integral converges is a segment of a line, $7/2 < a < 4$, with $b = 0$. On this convergent segment, we found a special solution, $(a, b) = (3.7, 0)$. This new solution is not far from the large-wavenumber asymptotic form of the Garrett–Munk spectrum, $(a, b) = (4, 0)$.

We have argued that there are two subdomains of power-law exponents that can yield quasi-steady solutions of the kinetic equation. For these ranges of exponents, the contribution of the scale-separated interactions

due to the IR and UV wavenumbers can be made to approximately balance each other. The Pelinovsky–Raevsky spectrum is a special case of this scenario.

The scenario, in which the energy spectrum in the inertial subrange is determined by the nonlocal interactions, provides an explanation for the variability of the power-law exponents of the observed spectra. They are a reflection of the variability of dominant players outside of the inertial range, such as the Coriolis effect, tides, and storms.

This possibility was further investigated by introducing rotation and then pursuing a rigorous asymptotic expansion of the kinetic equation. In doing so, we obtain the induced diffusion stationary states that appear as white lines in Fig. 6, which had previously been determined through a diffusive approximation. Much of the observed oceanic variability lies about these stationary states in the IR divergent subdomain.

A more detailed review of available observational data used for this study appears in PL. Numerical evaluation of the complete non-scale-invariant kinetic equation of the Garrett–Munk spectrum is presented in LPY in which we also consider waves that are slightly off resonant interactions. The theory, experimental data, and results of numerical simulations in Lvov and Yokoyama (2009) all hint at the importance of the IR contribution to the collision integral. The nonlocal interactions with large scales will therefore play a dominant role in forming the internal-wave spectrum. To the degree that the large scales are location dependent and not universal, the high-frequency, high-vertical-wavenumber internal-wave spectrum ought to be affected by this variability. Consequently, the internal-wave spectrum should be strongly dependent on the regional characteristics of the ocean, such as the local value of the Coriolis parameter and specific features of the spectrum, specifically for near-inertial frequencies.

Acknowledgments. This research is supported by NSF CMG Grants 0417724, 0417732 and 0417466. YL is also supported by NSF DMS Grant 0807871 and ONR Award N00014-09-1-0515. We are grateful to YITP in Kyoto University for allowing us to use their facility.

APPENDIX A

Asymptotics of Collision Integral in Infrared and Ultraviolet Limits

Let us integrate Eq. (18) over m_1 and m_2,

$$\frac{\partial n_{\mathbf{p}}}{\partial t} = \frac{1}{k}\int (T^0_{1,2} - T^1_{2,0} - T^2_{0,1})\, dk_1\, dk_2, \quad T^0_{1,2} = kk_1k_2|V^{\mathbf{p}}_{\mathbf{p}_1\mathbf{p}_2}|^2 f^{\mathbf{p}}_{\mathbf{p}_1\mathbf{p}_2} \Big/ (|g^{0'}_{1,2}|S^0_{1,2}),$$

$$g^{0'}_{1,2}(k_1,k_2) = \left.\frac{dg^0_{1,2}(m_1)}{dm_1}\right|_{m_1=m^*_1(k_1,k_2)}, \quad g^0_{1,2}(m_1) = \frac{k}{m} - \frac{k_1}{|m_1|} - \frac{k_2}{|m-m_1|}. \tag{A1}$$

Here, $g^{0'}_{1,2}$ appears because of $\delta_{\omega_{\mathbf{p}}-\omega_{\mathbf{p}_1}-\omega_{\mathbf{p}_2}}$, and $m^*_1(k_1, k_2)$ is given by the resonant conditions (21)–(23).

a. Infrared asymptotics

We consider the asymptotics of the integral in Eq. (A1) as $k_1 \to 0$. We employ the independent variables x and y, where $k_1 = kx$, $k_2 = k(1 + y)$, $x, y = O(\epsilon)$, $x > 0$, and $-x < y < x$. In this limit of $\epsilon \to 0$, $n_1 \gg n, n_2$. In this limit, Eqs. (21a) and (23b), Eqs. (21b) and (23a), and Eqs. (22a) and (22b) correspond to ES [Eqs. (25a) and (27b)], ID [Eqs. (25b) and (27a)], and PSI [Eqs. (25a) and (27b)], respectively. Without loss of generality, m is set to be positive.

Assuming the power-law spectrum of the wave action, $n(\mathbf{k}, m) = |\mathbf{k}|^{-a}|m|^{-b}$, we make Taylor expansion for the integrand of the kinetic Eq. (A1) as powers of ϵ: that is, x and y. Then, we get Table A1, which shows the leading orders of the each terms according to the asymptotics. The leading order of the collision integral is given by ID when $-3 < b < 3$. Therefore, we are going to show the procedure to get the leading order of ID (21b) and (23a) below.

TABLE A1. Asymptotics as $k_1 \to 0$. ES [(21a) and (23b)] gives ϵ^{-a+5} because of the symmetry of y. ID [(21b) and (23a)] gives $\epsilon^{-a-(b-7)/2}$ (ϵ^{-a+4}) because of the second cancellation. PSI [(22a) and (22b)] gives ϵ^{-a-b+5}. The asymptotics for $b = 0$ appear in parentheses.

Eq.	m_1	m_2	ω_1	ω_2	$V^{\mathbf{p}_i}_{\mathbf{p}_j\mathbf{p}_k}$	$f^{\mathbf{p}_i}_{\mathbf{p}_j\mathbf{p}_k}$	$g^{i'}_{j,k}$	$T^i_{j,k}$
(21a)	ϵ^0	ϵ^0	ϵ^1	ϵ^0	$\epsilon^{1/2}$	ϵ^{-a+1}	ϵ^0	ϵ^{-a+2}
(21b)	$\epsilon^{1/2}$	ϵ^0	$\epsilon^{1/2}$	ϵ^0	$\epsilon^{1/4}$	$\epsilon^{-a-(b-1)/2}$ (ϵ^{-a+1})	ϵ^0	$\epsilon^{-a-b//2+1}$ ($\epsilon^{-a+3/2}$)
(22a)	ϵ^1	ϵ^0	ϵ^0	ϵ^0	ϵ^1	ϵ^{-a-b}	ϵ^{-1}	ϵ^{-a-b+3}
(22b)	ϵ^1	ϵ^0	ϵ^0	ϵ^0	ϵ^1	ϵ^{-a-b}	ϵ^{-1}	ϵ^{-a-b+3}
(23a)	$\epsilon^{1/2}$	ϵ^0	$\epsilon^{1/2}$	ϵ^0	$\epsilon^{1/4}$	$\epsilon^{-a-(b-1)/2}$ (ϵ^{-a+1})	ϵ^0	$\epsilon^{-a-b//2+1}$ ($\epsilon^{-a+3/2}$)
(23b)	ϵ^0	ϵ^0	ϵ^1	ϵ^0	$\epsilon^{1/2}$	ϵ^{-a+1}	ϵ^0	ϵ^{-a+2}

As $\epsilon \to 0$, $n_2 \to n$ for ID solutions. Therefore, the leading order of $f^0_{1,2} \sim n_1(n_2 - n)$ and $f^2_{0,1} \sim n_1(n - n_2)$ is $O(\epsilon^{-a-(b-1)/2})$. The order $O(\epsilon^{-a-b/2})$ is canceled as $\epsilon \to 0$. This is called the first cancellation. It must be noted that the leading order when $b = 0$ is ½ larger than that when $b \neq 0$ because $\partial n/\partial m = 0$. The leading orders when $b = 0$ are written in parentheses in Table A1.

The leading order of the integrand in Eq. (A1) is written as

$$T^0_{1,2} - T^1_{2,0} - T^2_{0,1} \propto k^{-2a+3} m^{-2b+1} \frac{x^{-a-(b+1)/2} y}{\sqrt{(x+y)(x-y)}} \times \{-2ay^2 - b[(1-b)y(x+y) - 2x(x-y)] + b(b+1)xy\}. \quad \text{(A2)}$$

Therefore, the integrand has $O(\epsilon^{-a-(b-5)/2})$. The term that has $O(\epsilon^{-a-b/2+2})$ is canceled because $T^2_{0,1} \to T^0_{1,2}$ (and $T^1_{2,0} \to 0$) as $\epsilon \to 0$. This is the second cancellation.

Finally, we get the leading order of the kinetic equation after integration over y from $-x$ to x,

$$\frac{\partial n_{\mathbf{p}}}{\partial t} \propto -b(1-b)k^{4-2a} m^{1-2b} \int_0 x^{-a-(b-5)/2}\, dx. \quad \text{(A3)}$$

The integral has $O(\epsilon^{-a-(b-7)/2})$. Consequently, the integral converges if

$$a + (b-7)/2 < 0 \quad \text{and} \quad -3b3.$$

The integral for the PR spectrum, which gives $O(\epsilon^{-1/4})$, diverges as $k_1 \to 0$. However, the integral for the GM spectrum converges because $b = 0$ and the next order is $O(1)$.

It should be noted that the leading order when $b = 1$ is ½ larger than that when $b \neq 0, 1$ because a balance between first- and second-order derivative is made. The leading order when $b = 1$ is $O(\epsilon^{-a+7/2})$. It is also helpful to note that $T^0_{1,2} - T^1_{2,0} - T^2_{1,0} = O(\varepsilon^{-a+2})$ for ES because of no second cancellation. However, the collision integral has $O(\epsilon^{-a+5})$ because of symmetry of y. Therefore, the integral which is dominated by ES converges

$$a - 5 < 0 \quad \text{and} \quad b < -3.$$

Similarly, the integral that is dominated by PSI converges,

$$a + b - 5 < 0 \quad \text{and} \quad b > 3.$$

b. *Ultraviolet asymptotics*

Next, we consider the limit $k_1 \to \infty$. In this case, k_2 also approaches infinity. We employ the independent variables x and y as $k_1 = k/2[1 + (1/x) + y]$ and $k_2 = k/2[1 + (1/x) - y]$, where $x = O(\epsilon)$ and $-1 < y < 1$. Again, $m > 0$ is assumed.

TABLE A2. Asymptotics as $k_1 \to \infty$. PSI [(21a) and (21b)] gives ϵ^{a+b-3}. ES [(22a) and (23a)] gives ϵ^{a-3}. ID [(22b) and (23b)] gives $\epsilon^{a+b/2-4}$ ($\epsilon^{a-7/2}$). The asymptotics for $b = 0$ appear in parentheses.

Eq.	m_1	m_2	ω_1	ω_2	$V^{\mathbf{p}_i}_{\mathbf{p}_j\mathbf{p}_k}$	$f^{\mathbf{p}_i}_{\mathbf{p}_j\mathbf{p}_k}$	$g^{i'}_{j,k}$	$T^i_{j,k}$
(21a)	ϵ^{-1}	ϵ^{-1}	ϵ^0	ϵ^0	ϵ^0	ϵ^{a+b}	ϵ^1	ϵ^{a+b-2}
(21b)	ϵ^{-1}	ϵ^{-1}	ϵ^0	ϵ^0	ϵ^0	ϵ^{a+b}	ϵ^1	ϵ^{a+b-2}
(22a)	ϵ^0	ϵ^0	ϵ^{-1}	ϵ^{-1}	ϵ^{-1}	ϵ^a	ϵ^{-1}	ϵ^{a-2}
(22b)	$\epsilon^{-1/2}$	$\epsilon^{-1/2}$	$\epsilon^{-1/2}$	$\epsilon^{-1/2}$	ϵ^{-1}	$\epsilon^{a+b/2+1}$ ($\epsilon^{a+3/2}$)	$\epsilon^{1/2}$	$\epsilon^{a+b/2-3}$ ($\epsilon^{a-5/2}$)
(23a)	ϵ^0	ϵ^0	ϵ^{-1}	ϵ^{-1}	ϵ^{-1}	ϵ^a	ϵ^{-1}	ϵ^{a-2}
(23b)	$\epsilon^{-1/2}$	$\epsilon^{-1/2}$	$\epsilon^{-1/2}$	$\epsilon^{-1/2}$	ϵ^{-1}	$\epsilon^{a+b/2+1}$ ($\epsilon^{a+3/2}$)	$\epsilon^{1/2}$	$\epsilon^{a+b/2-3}$ ($\epsilon^{a-5/2}$)

The leading orders are obtained by the similar manner used in the IR asymptotic and are summarized in Table A2. The leading order of the integral is given by ID, whose wavenumbers are given by Eqs. (22b) and (23b), when $-2 < b < 2$. In this limit, no second cancellation is made.

As the result of the perturbation theory, we get the leading order,

$$\frac{\partial n_{\mathbf{p}}}{\partial t} \propto k^{4-2a} m^{1-2b} b \int_0 x^{a+b/2-5}\, dx. \quad \text{(A4)}$$

It has $O(\epsilon^{a+b/2-4})$. Therefore, the integral converges if

$$a + b/2 - 4 > 0 \quad \text{and} \quad -2 < b < 2.$$

The integral for the PR spectrum, which gives $O(\epsilon^{-1/4})$, diverges as $k_1 \to \infty$. The integral for the Garrett–Munk spectrum, which gives $O(\epsilon^0)$, converges because $b = 0$.

Similarly,

$$\frac{\partial n_{\mathbf{p}}}{\partial t} \propto -k^{4-2a} m^{1-2b} b \int_0 x^{a-2}\, dx \quad \text{(A5)}$$

for ES, which is dominant for $b > 2$. Consequently, the integral converges also if

$$a - 3 > 0 \quad \text{and} \quad b > 2.$$

In the same manner, the convergent domain of the integral for PSI is given by

$$a + b - 3 > 0 \quad \text{and} \quad b < -2.$$

APPENDIX B

Frequency–Vertical-Wavenumber and Horizontal–Vertical-Wavenumber Spectrum

The theoretical work presented below addresses the asymptotic power laws of a three-dimensional action

spectrum. To connect with that work, note that a horizontally isotropic power-law form of the three-dimensional wave action $n(\mathbf{k}, m)$ is given by Eq. (2).

The corresponding vertical wavenumber–frequency spectrum of energy is obtained by transforming $n_{\mathbf{k},m}$ from wavenumber space $(\mathbf{k}, m)$ to the vertical wavenumber–frequency space (ω, m) and multiplying by frequency. In the high-frequency, large-wavenumber limit,

$$E(m,\omega) \propto \omega^{2-a} m^{2-a-b}.$$

The total energy density of the wave field is then

$$E = \int \omega(\mathbf{k},m) n(\mathbf{k},m)\, d\mathbf{k}\, dm = \int E(\omega,m)\, d\omega\, dm.$$

Thus, we also find it convenient to work with the wave action spectrum expressed as a function of ω and m Therefore, we also introduced (37). The relation between a, b and $\tilde{a}, \tilde{b}$ reads as

$$\tilde{a} = -a, \quad \tilde{b} = -a - b.$$

APPENDIX C

Asymptotic Expansion for Small f Values

In this section, we perform the small f calculations of section 6. We start from the kinetic equation written as Eq. (40). There we change variables in the first line of Eq. (40) as

$$m_1 = E_3(\omega_1) + \mu[E_1(\omega_1) - E_3(\omega_1)]$$

and in the second line of Eq. (40) as

$$m_1 = E_3(\omega_1) + \mu[E_2(\omega_1) - E_3(\omega_1)].$$

Then, Eq. (40) becomes the following form:

$$\frac{\partial}{\partial t} n[k(\omega,m),m] = \frac{2}{k}\int_f^{f+\omega_s} d\omega_1 \int_0^1 d\mu \mathcal{P}_1 - \frac{2}{k}\int_{\omega-f-\omega_s}^{\omega-f} d\omega_1 \int_0^1 d\mu \mathcal{P}_2. \quad \text{(C1)}$$

Here, we introduced integrands $\mathcal{P}_1$ and $\mathcal{P}_2$ to be

$$\mathcal{P}_1 = J\frac{|V^0_{1,2}|^2}{S^0_{1,2}} n_1(n_2 - n)[E_1(\omega_1) - E_3(\omega_1)] \quad \text{and}$$

$$\mathcal{P}_2 = J\frac{|V^0_{1,2}|^2}{S^0_{1,2}} n_2(n - n_1)[E_2(\omega_1) - E_3(\omega_1)]. \quad \text{(C2)}$$

Before proceeding, note the following symmetries:

$$E_1(\omega_1 = \omega - \omega_1') = m - E_2(\omega_1'),$$

$$E_3(\omega_1 = \omega - \omega_1') = m - E_3(\omega_1'), \quad \text{and}$$

$$E_4(\omega_1 = \omega - \omega_1') = m - E_4(\omega_1').$$

These symmetries explain why two disconnected regions on Fig. 5 look like mirrored and shifted copies of each other. These symmetries further allow us simplification of evaluation of ID contribution by noticing that the contribution from ID1 is equal to the contribution from ID3. To quantify the contribution of near-inertial waves to a (ω, m) mode, we write

$$\epsilon \sim f \ll \omega = 1.$$

Subsequently, in the domain ID3 we write

$$\omega_1 = f + \epsilon,$$

in $\mathcal{P}_1$ and in the domain ID2 we write

$$\omega_1 = \omega + f + \epsilon$$

in $\mathcal{P}_2$. Furthermore, we expand $\mathcal{P}_1$ and $\mathcal{P}_2$ in powers of ϵ and f without making any assumptions of the relative smallness of f and ϵ. We use the facts that

$$m > 0, \quad \epsilon > 0, \quad f > 0, \quad \text{and} \quad 0 < \mu < 1.$$

Define

$$\mathcal{P}_1 = P_1 + P_2 \quad \text{and}$$

$$\mathcal{P}_2 = P_3 + P_4.$$

This allows us to expand P_1, P_2, P_3, and P_4 in powers of f and ϵ. We perform these calculations analytically on Mathematica software. Mathematica was then able to perform the integrals of $\mathcal{P}_1$ and $\mathcal{P}_2$ over μ from 0 to 1 in Eq. (C1) analytically. The result is given by Eq. (41).

REFERENCES

Anderson, S., 1992: Shear, strain, and thermohaline vertical fine structure in the upper ocean. Ph.D. thesis, University of California, San Diego, 155 pp.

Broutman, D., J. W. Rottman, and S. D. Eckermann, 2004: Ray methods for internal waves in the atmosphere and ocean. *Annu. Rev. Fluid Mech.,* **36,** 233–253.

Caillol, P., and V. Zeitlin, 2000: Kinetic equations and stationary energy spectra of weakly nonlinear internal gravity waves. *Dyn. Atmos. Oceans,* **32,** 81–112.

Cairns, J. L., and G. O. Williams, 1976: Internal wave observations from a midwater float, 2. *J. Geophys. Res.,* **81,** 1943–1950.

Chereskin, T. K., M. Y. Mooris, P. P. Niiler, P. M. Kosro, R. L. Smith, S. R. Ramp, C. A. Collins, and D. L. Musgrave, 2000: Spatial and temporal characteristics of the mesoscale circulation of the California Current from eddy-resolving moored and shipboard measurements. *J. Geophys. Res.,* **105,** 1245–1269.

Cushman-Roisin, B., 1994: *Introduction to Geophysical Fluid Dynamics*. Prentice-Hall, 320 pp.

D'Asaro, E. A., 1984: Wind forced internal waves in the North Pacific and Sargasso Sea. *J. Phys. Oceanogr.,* **14,** 781–794.

——, 1995: A collection of papers on the ocean storms experiment. *J. Phys. Oceanogr.,* **25,** 2817–2818.

——, and M. D. Morehead, 1991: Internal waves and velocity fine structure in the Arctic Ocean. *J. Geophys. Res.,* **96,** 12 725–12 738.

Eriksen, C., D. Rudnick, R. Weller, R. T. Pollard, and L. Regier, 1991: Ocean frontal variability in the Frontal Air-Sea Interaction Experiment. *J. Geophys. Res.,* **96,** 8569–8591.

Flatté, S. M., F. S. Henyey, and J. A. Wright, 1985: Eikonal calculations of short-wavelength internal-wave spectra. *J. Geophys. Res.,* **90,** 7265–7272.

Foffonoff, N. P., 1969: Spectral characteristics of internal waves in the ocean. *Deep-Sea Res.,* **16,** 58–71.

Garrett, C. J. R., and W. H. Munk, 1972: Space-time scales of internal waves. *Geophys. Fluid Dyn.,* **3,** 225–264.

——, and ——, 1975: Space-time scales of internal waves: A progress report. *J. Geophys. Res.,* **80,** 281–297.

——, and ——, 1979: Internal waves in the ocean. *Annu. Rev. Fluid Mech.,* **11,** 339–369.

Gregg, M. C., H. E. Seim, and D. B. Percival, 1993: Statistics of shear and turbulent dissipation profiles in random internal wave fields. *J. Phys. Oceanogr.,* **23,** 1777–1799.

Hasselmann, K., 1966: Feynman diagrams and interaction rules of wave-wave scattering processes. *Rev. Geophys.,* **4,** 1–32.

Henyey, F. S., J. Wright, and S. M. Flatté, 1986: Energy and action flow through the internal wave field: An eikonal approach. *J. Geophys. Res.,* **91,** 8487–8495.

Keffer, T., 1983: The baroclinic stability of the Atlantic North Equatorial Current. *J. Phys. Oceanogr.,* **13,** 624–631.

Kenyon, K. E., 1966: Wave-wave scattering for gravity waves and Rossby waves. Ph.D. thesis, University of California, San Diego, 93 pp.

——, 1968: Wave-wave interactions of surface and internal waves. *J. Mar. Res.,* **26,** 208–231.

Kuznetsov, E. A., 1972: On turbulence of ion sound in plasma in a magnetic field. *Zh. Eksper. Teoret. Fiz,* **62,** 584–592.

Levine, M. D., J. D. Irish, T. E. Ewart, and S. A. Reynolds, 1986: Simultaneous spatial and temporal measurements of the internal wavefield during MATE. *J. Geophys. Res.,* **91,** 9709–9719.

——, C. A. Paulson, and J. H. Morison, 1987: Observations of internal gravity waves under the arctic pack ice. *J. Geophys. Res.,* **92,** 779–782.

Lvov, Y. V., and E. G. Tabak, 2001: Hamiltonian formalism and the Garrett–Munk spectrum of internal waves in the ocean. *Phys. Rev. Lett.,* **87,** 168501, doi:10.1103/PhysRevLett.87.168501.

——, and S. Nazarenko, 2004: Noisy spectra, long correlations, and intermittency in wave turbulence. *Phys. Rev.,* **69,** 66 608.

——, and E. G. Tabak, 2004: A Hamiltonian formulation for long internal waves. *Physica D,* **195,** 106–122.

——, and N. Yokoyama, 2009: Nonlinear wave-wave interactions in stratified flows: Direct numerical simulations. *Physica D,* **238,** 803–815.

——, K. L. Polzin, and E. G. Tabak, 2004: Energy spectra of the ocean's internal wave field: Theory and observations. *Phys. Rev. Lett.,* **92,** 128501, doi:10.1103/PhysRevLett.92.128501.

McComas, C. H., and F. P. Bretherton, 1977: Resonant interaction of oceanic internal waves. *J. Geophys. Res.,* **82,** 1397–1412.

——, and P. Müller, 1981: Time scales of resonant interactions among oceanic internal waves. *J. Phys. Oceanogr.,* **11,** 139–147.

Milder, D. M., 1990: The effects of truncation on surface-wave Hamiltonian. *J. Fluid Mech.,* **216,** 249–262.

Müller, P., and D. J. Olbers, 1975: On the dynamics of internal waves in the deep ocean. *J. Geophys. Res.,* **80,** 3848–3860.

——, ——, and J. Willebrand, 1978: The IWEX spectrum. *J. Geophys. Res.,* **83,** 479–500.

——, G. Holloway, F. Henyey, and N. Pomphrey, 1986: Nonlinear interactions among internal gravity waves. *Rev. Geophys.,* **24,** 493–536.

Olbers, D. J., 1974: On the energy balance of small scale internal waves in the deep sea. Hamburger geophysikalische Einzelschriften 27, 102 pp.

——, 1976: Nonlinear energy transfer and the energy balance of the internal wave field in the deep ocean. *J. Fluid Mech.,* **74,** 375–399.

Pelinovsky, E. N., and M. A. Raevsky, 1977: Weak turbulence of the internal waves of the ocean. *Izv. Acad. Sci. USSR Atmos. Oceanic Phys.,* **13,** 187–193.

Polzin, K. L., 2004: A heuristic description of internal wave dynamics. *J. Phys. Oceanogr.,* **34,** 214–230.

——, E. Kunze, J. M. Toole, and R. W. Schmitt, 2003: The partition of finescale energy into internal waves and subinertial motions. *J. Phys. Oceanogr.,* **33,** 234–248.

Pomphrey, N., J. D. Meiss, and K. M. Watson, 1980: Description of nonlinear internal wave interactions using Langevin methods. *J. Geophys. Res.,* **85,** 1085–1094.

Schmitt, R. W., J. R. Ledwell, E. T. Montgomery, K. L. Polzin, and J. M. Toole, 2005: Enhanced diapycnal mixing by salt fingers in the thermocline of the tropical Atlantic. *Science,* **308,** 685–688.

Sherman, J. T., and R. Pinkel, 1991: Estimates of the vertical wavenumber–frequency spectra of vertical shear and strain. *J. Phys. Oceanogr.,* **21,** 292–303.

Silverthorne, K. E., and J. M. Toole, 2009: Seasonal kinetic energy variability of near-inertial motions. *J. Phys. Oceanogr.,* **39,** 1035–1049.

Voronovich, A. G., 1979: Hamiltonian formalism for internal waves in the ocean. *Izv. Acad. Sci. USSR Atmos. Oceanic Phys.,* **15,** 52–57.

Weller, R. A., K. L. Polzin, D. L. Rundnick, C. C. Eriksen, and N. S. Oakey, 1991: Forced ocean response during the Frontal Air-Sea Interaction Experiment. *J. Geophys. Res.,* **96,** 8611–8638.

——, P. W. Furey, M. A. Spall, and R. E. Davis, 2004: The large-scale context for oceanic subduction in the northeast Atlantic. *Deep-Sea Res. I,* **51,** 665–699.

Zakharov, V. E., 1967: The instability of waves in nonlinear dispersive media. *Sov. Phys. JETP,* **24,** 740–744.

——, 1968: Stability of periodic waves of finite amplitude on the surface of a deep fluid. *J. Appl. Mech. Tech. Phys.,* **2,** 190–194.

——, V. S. L'vov, and G. Falkovich, 1992: *Kolmogorov Spectra of Turbulence I: Wave Turbulence*. Springer-Verlag, 246 pp.